Available online at www.sciencedirect.com
SCIENCE DIRECT®
Biomaterials 26 (2005) 4856–4865
Biomaterials
www.elsevier.com/locate/biomaterials

Enhanced osteoinduction by controlled release of bone morphogenetic protein-2 from biodegradable sponge composed of gelatin and β-tricalcium phosphate

Yoshitake Takahashi, Masaya Yamamoto, Yasuhiko Tabata*

Department of Biomaterials, Field of Tissue Engineering, Institute for Frontier Medical Sciences, Kyoto University, 53 Kawara-cho Shogoin, Sakyo-ku, Kyoto 606-8507, Japan

Received 4 September 2004; accepted 5 January 2005

Abstract

Biodegradable gelatin sponges at different contents of β-tricalcium phosphate (β-TCP) were fabricated to allow bone morphogenetic protein (BMP)-2 to incorporate into them. The in vivo osteoinduction activity of the sponges incorporating BMP-2 was investigated, while their in vivo profile of BMP-2 release was evaluated. The sponges prepared had an interconnected pore structure with an average pore size of 200 μm, irrespective of the β-TCP content. The in vivo release test revealed that BMP-2 was released in vivo at a similar time profile, irrespective of the β-TCP content. The in vivo time period of BMP-2 retention was longer than 28 days. When the osteoinduction activity of gelatin or gelatin–β-TCP sponges incorporating BMP-2 was studied following the implantation into the back subcutis of rats in terms of histological and biochemical examinations, homogeneous bone formation was histologically observed throughout the sponges, although the extent of bone formation was higher in the sponges with the lower contents of β-TCP. On the other hand, the level of alkaline phosphatase activity and osteocalcin content at the implanted sites of sponges decreased with an increase in the content of β-TCP. The gelatin sponge exhibited significantly higher osteoinduction activity than that of any gelatin–β-TCP sponge, although every sponge with or without β-TCP showed a similar in vivo profile of BMP-2 release. In addition, the in vitro collagenase digestion experiments revealed that the gelatin–β-TCP sponge collapsed easier than the gelatin sponge without β-TCP incorporation. These results suggest that the maintenance of the intrasponge space necessary for the osteoinduction is one factor contributing to the osteoinduction extent of BMP-2-incorporating sponges.

Keywords: Bone morphogenetic protein; Gelatin–β-TCP sponge; Controlled release; Osteoinduction

1. Introduction

Bone defects that are generated by tumor resection, trauma, and congenital abnormality have been clinically treated by the implantation of bioceramics or autogenous and allogenous bone grafts. Although autografting is a popular procedure for reconstructive surgery, it has several disadvantages, such as the shortage of donor supply, the persistence of pain, the nerve damage, fracture, and cosmetic disability at the donor site. On the other hand, there are no donor site problems for allografting, while allografting has some clinical risks including disease transmission and immunological reaction [1]. As one trial to overcome the problems, bone tissue engineering has been attracted much attention as a new therapeutic technology which induces bone regeneration by making use of osteoinductive growth factors, osteogenic cells, and scaffolds or their combination [2]. It is no doubt that a combination of osteoinductive growth factors and scaffolds provides an appropriate osteoinductive environment for osteogenic cells.

*Corresponding author. Tel.: +81 75 751 4121; fax: +81 75 751 4646.
E-mail address: yasuhiko@frontier.kyoto-u.ac.jp (Y. Tabata).

0142-9612/$ - see front matter © 2005 Elsevier Ltd. All rights reserved.
doi:10.1016/j.biomaterials.2005.01.012

Osteoinductive growth factors, such as bone morphogenetic protein (BMP), transforming growth factor-β (TGF-β), and basic fibroblast growth factor (bFGF), have been investigated to induce bone regeneration in the body [3]. Among them, BMP-2 and BMP-7 (OP-1) have already been applied clinically for bone regeneration at the bone defect, because of their high osteoinduction activity [4,5]. However, the BMP administrated in the solution form does not always expect the in vivo satisfied efficacy in bone regeneration. Therefore, it is necessary to develop a carrier for the controlled release of biologically active BMPs over an extended time period.

Gelatin is a denatured collagen and commercially available as a biodegradable polymer. It has been extensively utilized for pharmaceutical and medical purposes, and its biosafety has been proven through the long clinical applications [6]. Other advantages of gelatin are the easiness of chemical modification and the commercial availability of samples with different physicochemical properties. We have prepared a biodegradable hydrogel of gelatin for the controlled release of BMP to succeed in inducing bone regeneration [7]. On the other hand, it has been experimentally demonstrated from some researches that the attachment and proliferation of cells on substrates are promoted by the surface coating of gelatin [8–10]. These findings suggest that gelatin is one of the materials compatible to cells.

Since it is preferable that the scaffolds for bone regeneration basically function as the substrate for the attachment and proliferation of osteogenic cells, three-dimensional biodegradable materials with a porous structure, such as glycolide–lactide copolymer nonwoven fabrics, collagen sponges, and calcium phosphate ceramics, have been used [11,12]. Among them, hydroxyapatite (HAp) and β-tricalcium phosphate (β-TCP) of bioactive ceramics have been extensively investigated as the cell scaffold for bone tissue engineering [11–22] because it is well recognized that they are compatible to natural bone tissue. However, since HAp is not practically degraded under the physical condition, it remains inside the bone tissue regenerated. Therefore, as one trial to improve the in vivo poor degradability, HAp has been attempted to mix with organic materials of collagen and glycolide–lactide copolymer. The combination was effective in manipulating the degradation and mechanical properties for the HAp scaffolds [23–28]. β-TCP is advantageous from the viewpoint of material biodegradability, though brittle compared with HAp. On the other hand, some research groups have investigated the osteoinduction of BMP-incorporating composites for different animal models. However, little has been demonstrated on the effect of the bioceramic content on the osteoinduction activity [29–35].

Naturally occurring bone matrix provides an environment favorable for the in vivo osteoinduction in terms of the bone cell scaffold and growth factor delivery vehicle. In this study, as a mimic of the natural bone matrix, we have designed a biodegradable cell scaffold of organic–inorganic composite combined with the controlled release nature of BMP. Biodegradable gelatin sponges at different contents of β-TCP were fabricated. Following incorporation of BMP-2 into the gelatin–β-TCP sponges, their in vivo BMP-2 release from the sponges was investigated. To obtain fundamental information on in vivo osteoinductivity of gelatin–β-TCP sponges incorporating BMP-2, the in vivo osteoinduction activity of gelatin–β-TCP sponges incorporating BMP-2 was assessed at the back subcutis of rats in terms of the β-TCP content.

2. Materials and methods

2.1. Materials

A gelatin sample with an isoelectric point (IEP) of 9.0 was prepared through an acidic process of porcine skin collagen type I (Nitta Gelatin Co., Osaka, Japan). β-TCP granules (2 μm in average diameter) were obtained from Taihei Chemical Industries, Nara, Japan. $Na^{125}I$ (740 MBq/ml in 0.1 N NaOH aqueous solution) was purchased from NEN Research Products, Du Pont, Wilmington, USA. Collagenase was purchased from Sigma Chemical Co., St. Louis, MO, USA. Other chemicals were obtained from Wako Pure Chemical Industries, Osaka, Japan and used without further purification.

2.2. Preparation of gelatin sponges with or without β-TCP

Gelatin sponges incorporating β-TCP (gelatin–β-TCP sponges) were prepared by chemical cross-linking of gelatin with glutaraldehyde in the presence of β-TCP granules at different amounts (Table 1). Briefly, 4.29 wt% aqueous solution of gelatin at different contents of β-TCP (70 ml) was mixed at 5000 rpm at 37 °C for 3 min by using a homogenizer (ED-12, Nihonseiki Co., Tokyo, Japan). After addition of 2.17 wt% of glutaraldehyde aqueous solution (30 ml), the mixed solution was further mixed for 15 s by the homogenizer. The resulting solution was cast into a polypropylene dish of $138 \times 138\,cm^2$ and 5 mm depth, followed by leaving at 4 °C for 12 h for gelatin cross-linking. Then, the cross-linked gelatin hydrogels with or without β-TCP were placed into 100 mM of aqueous glycine solution at 37 °C for 1 h to block the residual aldehyde groups of glutaraldehyde. Following complete washing with double distilled water (DDW), the hydrogels were freeze-dried and cut into cubes of $5 \times 5 \times 5\,mm^3$.

Table 1
Characterization of gelatin sponges incorporating various amounts of β-TCP prepared

β-TCP content (wt%)	Pore size (μm)	Porosity (%)	Compression modulus (MPa)
0	184.9±58.2	96.6	0.27±0.01
25	198.2±52.3	96.2	0.52±0.14
50	179.1±27.8	95.9	1.13±0.13
75	185.5±62.4	95.4	2.60±0.32
90	178.2±50.0	95.1	4.97±0.73

The resulting sponges were sputter-coated with gold/palladium and viewed both on a scanning electron microscope (SEM, S-2380N, HITACHI, Japan) and a field emission SEM with energy dispersive X-ray (EDX) microanalyzer (JSM 6500F, JEOL, Japan). The average pore size and porosity of sponges were measured by the methods reported previously (Table 1) [36,37].

2.3. *In vitro compression resistance of gelatin and gelatin–β-TCP sponges*

The in vitro compression resistance of gelatin and gelatin–β-TCP sponges in the freeze-dried state was evaluated by measuring their compression moduli at a rate of 1 mm/min (AG-5000B, Shimadzu, Kyoto, Japan). The load-deformation curve was obtained and the compression modulus of sponges was calculated from the initial slope of load-deformation curve. Measurement was done five times for each sample to calculate the average value ± the standard deviation of the mean.

2.4. *Radioiodination of BMP-2*

Human recombinant BMP-2 (Yamanouchi Pharmaceutical Co., Japan) was radioiodinated according to the method of Greenwood et al. [38]. Briefly, 4 μl of $Na^{125}I$ solution was added to 40 μl of 1 mg/ml BMP-2 solution containing 5 mM glutamic acid, 2.5 wt% glycine, 0.5 wt% sucrose, and 0.01 wt% Tween 80 (pH 4.5). Then, 0.2 mg/ml of chloramine-T potassium phosphate-buffered solution (0.5 M, pH 7.5) containing 0.5 M sodium chloride (100 μl) was added to the solution mixture. After agitation at room temperature for 2 min, 100 μl of phosphate-buffered saline solution (PBS, pH 7.5) containing 0.4 mg of sodium metabisulfate was added to the reaction solution to stop the radioiodination. The reaction mixture was passed through an anionic-exchange column to remove the uncoupled, free ^{125}I molecules from the ^{125}I-labeled BMP-2.

2.5. *Preparation of gelatin and gelatin–β-TCP sponges incorporating BMP-2*

To prepare gelatin and gelatin–β-TCP sponges incorporating BMP-2, 20 μl of aqueous solution containing BMP-2 (0.25 μg/μl) or ^{125}I-labeled BMP-2 (0.03 μg/μl) was dropped onto the freeze-dried sponge, followed by leaving it at 4 °C overnight. The resulting sponge was used as the gelatin and gelatin–β-TCP sponges incorporating BMP-2 without washing. Similarly, 20 μl of BMP-2-free PBS was impregnated into gelatin and gelatin–β-TCP sponges to obtain respective BMP-2-free, empty sponges.

2.6. *In vivo evaluation of BMP-2 release from gelatin and gelatin–β-TCP sponges*

Gelatin and gelatin–β-TCP sponges incorporating ^{125}I-labeled BMP-2 were implanted into the back subcutis of 6-week-age female ddY mice (Shimizu Laboratory Supply Inc., Japan) at the central position 15 mm away from their tail root. At different time intervals, the mouse skin including the implanted site of sponge ($3 \times 5\,cm^2$) was excised and the corresponding facia was thoroughly wiped off with a filter paper to absorb ^{125}I-labeled BMP-2. The radioactivity of the gelatin sponge remained, the skin strip excised, and the filter paper was measured on a gamma counter (ARC-301B, Aloka Co., Ltd., Japan) to assess the time profile of in vivo BMP-2 retention. The radioactivity was divided by the original radioactivity of gelatin and gelatin–β-TCP sponges incorporating ^{125}I-labeled BMP-2 to calculate the percent remaining of BMP-2. All the radioactivities were compensated for the natural decay of ^{125}I. Experimental group was composed of three mice unless otherwise mentioned.

2.7. *Histological evaluation of bone tissue ectopically induced by gelatin and gelatin–β-TCP sponges incorporating BMP-2*

Gelatin and gelatin–β-TCP sponges incorporating 5.0 μg of BMP-2 were implanted into the back subcutis

of Fisher F344 rats (Shimizu Laboratory Supply Inc., Japan). The BMP-2-free, empty sponge was used as a control. The subcutaneous tissue including gelatin and gelatin–β-TCP sponges with or without BMP-2 incorporation was fixed in 10 wt% neutral-buffered formalin solution 4 weeks after implantation. The tissue samples fixed were conventionally dehydrated in aqueous solutions of ethanol at sequentially increasing concentrations of 70–100 vol%, immersed in xylene, and embedded in paraffin. The samples were sectioned at 4 μm thickness and stained by hematoxylin and eosin (H&E) to view on an optical microscope (AX-80, OLYMPUS, Japan).

2.8. Biochemical evaluation of BMP-2-induced ectopic bone formation

The samples obtained 2 and 4 weeks after implantation were freeze-dried and grinded. The grinded sample (5 mg) was homogenized in 1 ml of mixed aqueous solution of 0.2% Nonidet P-40, 10 mM Tris–HCl, and 1 mM $MgCl_2$ (pH 7.5). The homogenate was centrifuged at 12,000 rpm and 4 °C for 15 min and the alkaline phosphatase (ALP) activity of supernatant obtained was determined by a *p*-nitro-phenyl-phosphate method [39].

For the determination of osteocalcin content, the grinded sample (5 mg) was placed for 12 h in 40% formic acid aqueous solution (1 ml) for decalcification. During the decalcification process, the non-collagenous proteins of bone matrix were extracted. After desalting of the extracts with a gel filtration using Sephadex™ G-25M column (PD-10, Amersham Pharmacia Biotech AB, Sweden), the resulting solution was freeze-dried and subjected to an osteocalcin rat enzyme-linked immunosorbent assay (ELISA) (rat osteocalcin ELISA system, Amersham Biosciences, Tokyo, Japan) [39].

2.9. Enzymatic degradation of gelatin and gelatin–β-TCP sponges

Gelatin and gelatin–β-TCP sponges were immersed in Tris buffer (pH 7.4) containing 5 U/ml of collagenase at 37 °C and then washed with distilled water. Appearance of the sponges was observed by an optical microscope.

2.10. Statistical analysis

All the data were shown as the mean value ± the standard deviation of the mean. The pairwise comparisons of individual group means were conducted based on the one-way ANOVA. Values of $p<0.05$ were considered statistically significant.

3. Results

3.1. Characterization of gelatin and gelatin–β-TCP sponges

Fig. 1 shows the electron microscopic structure and EDX image of gelatin and gelatin–β-TCP sponges. Irrespective of the β-TCP content, the similar intrastructure of sponges was observed. Every sponge had an interconnected-porous structure with the pore size range of 180–200 μm and the porosity around 96% (Table 1). β-TCP granules were homogeneously localized in the gelatin walls of the sponges, while the intensity of the peak for CaKα X-ray depends on the β-TCP content (Figs. 1k–o). On the other hand, the compression modulus of sponges increased with an increase in the content of β-TCP.

3.2. In vivo evaluation of BMP-2 release from gelatin and gelatin–β-TCP sponges incorporating BMP-2

Fig. 2 shows the in vivo decrement patterns of the remaining radioactivity at the implanted site of gelatin and gelatin–β-TCP sponges incorporating ^{125}I-labeled BMP-2. The period of BMP-2 retention was not influenced by the β-TCP content. Negligibly low radioactivity was detected in the thyroid gland for each experimental group, indicating no release of free radioactive iodine from ^{125}I-labeled BMP-2 (data not shown).

3.3. Ectopic bone formation induced by gelatin and gelatin–β-TCP sponges incorporating BMP-2

Fig. 3 shows the histological section of subcutaneous tissue 4 weeks after implantation of gelatin and gelatin–β-TCP sponges incorporating BMP-2. Every BMP-2-incorporated sponge induced bone formation homogeneously throughout the sponges, although the extent of bone formation was higher in the sponges with the lower contents of β-TCP.

Irrespective of the β-TCP incorporation, the gelatin and gelatin–β-TCP sponges incorporating BMP-2 enhanced the ALP activity to a significantly higher extent than that of the BMP-2-free sponges (Fig. 4a). The highest ALP activity was observed for the gelatin sponge without β-TCP. The similar β-TCP content dependency was observed for the osteocalcin content of subcutaneous tissues around the implanted site of sponges incorporating BMP-2. The BMP-2-incorporated gelatin sponge without β-TCP exhibited the highest osteocalcin content 4 weeks after the implantation, while the osteocalcin content decreased with the increasing content of β-TCP (Fig. 4b). Incorporation of BMP-2 enabled gelatin sponges to enhance the induction activity of bone formation, irrespective of the β-TCP incorporation.

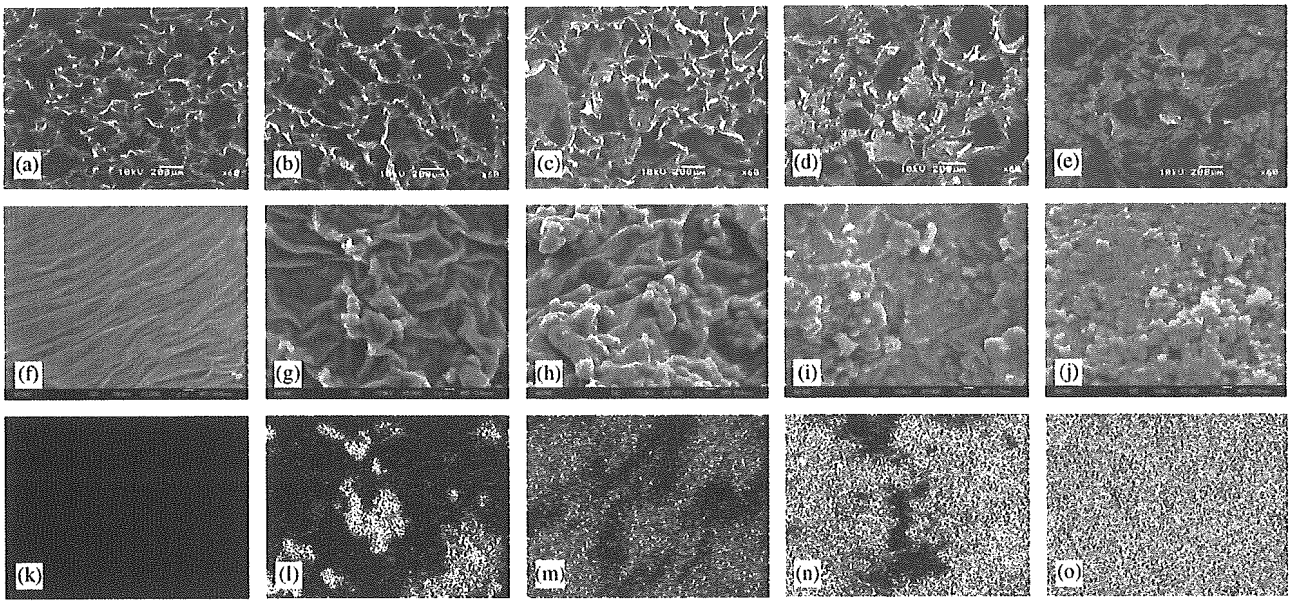

Fig. 1. Scanning electron micrographs of gelatin sponges incorporating 0 (a, f), 25 (b, g), 50 (c, h), 75 (d, i), and 90 wt% of β-TCP (e, j) at the magnifications of 60 (a–e) and 5000 (f–j). EDX images of calcium element for gelatin sponges incorporating 0 (k), 25 (l), 50 (m), 75 (n), and 90 wt% of β-TCP (o) at a magnification of 5000.

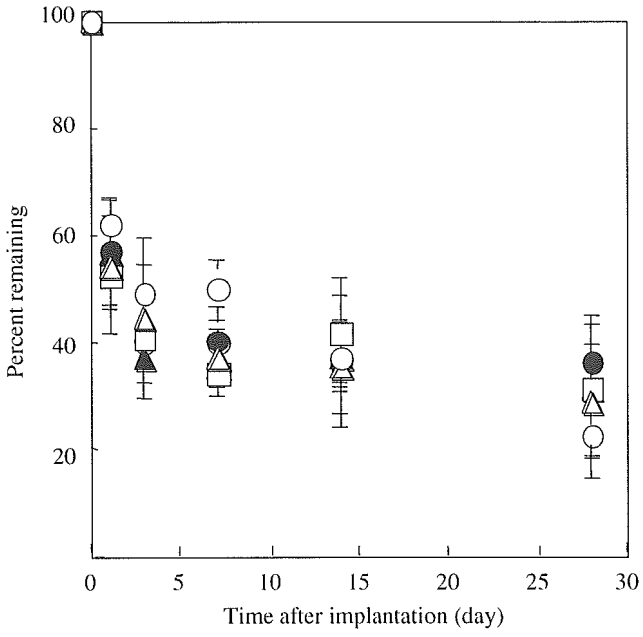

Fig. 2. In vivo time profiles of the radioactivity remaining after the subcutaneous implantation of gelatin–β-TCP sponges incorporating ^{125}I-labeled BMP-2 into the back of mice. The β-TCP contents of gelatin sponges are 0 (○), 25 (△), 50 (□), 75 (●), and 90 wt% (▲).

4. Discussion

The present study demonstrates that the in vivo osteoinductive activity of gelatin–β-TCP sponges incorporating BMP-2 was greatly influenced by the β-TCP content. In our previous studies, the hydrogel of gelatin in different shapes, such as disks, sheets, and microspheres, could be fabricated to function as the release carrier of various growth factors [40]. Although it is known that gelatin is one of the substrate materials for cell adhesion and proliferation, the hydrogel dose not always function as a good scaffold of migration, proliferation, and differentiation of cells, because of no porous structure necessary for cell infiltration. Therefore, in this study, a hydrogel with a porous sponge structure was fabricated by a homogenization process of aqueous gelatin solution. This homogenization process has been reported to prepare a synthetic dermal substitute of collagen [41]. The pore size was adjusted at 180–200 μm since the pore size suitable for cell infiltration and ingrowth of host bone tissue is reported to be in the range of 100–350 μm [42,43]. As a result, the gelatin sponge obtained functions not only as the release carrier for growth factor, but also as the scaffold of cell attachment and proliferation. For the sponge preparation, β-TCP which has been extensively explored as one bioactive substrate was combined. Since spontaneous gelation of gelatin solution homogeneously dispersing various amounts of β-TCP takes place immediately after leaving them at 4 °C, no sedimentation of β-TCP granules was observed in this study. Homogeneous incorporation of β-TCP enabled the gelatin sponge to increase the compression modulus without any change in the pore structure. The mechanical resistance of sponges against compression in a dry state increased with the increased β-TCP content (Table 1). The scaffold of sponge shape has been used for cell scaffold from the viewpoint of good nutrients and oxygen supply to cells and superior cell infiltration.

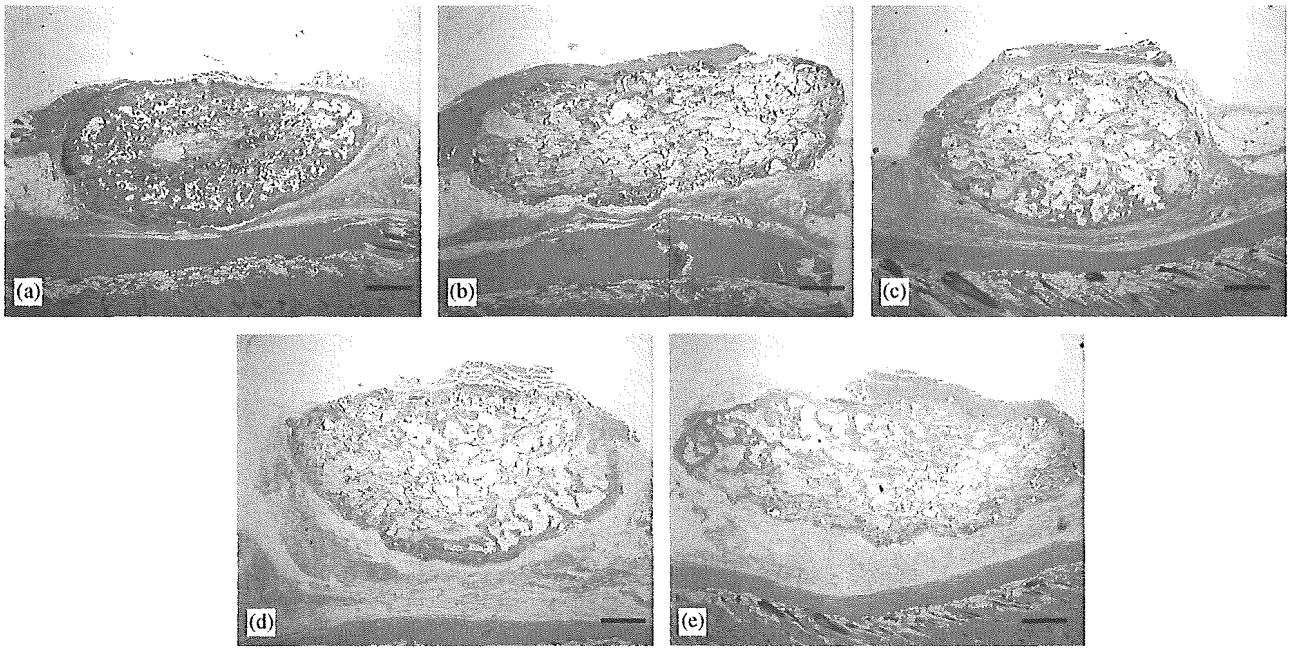

Fig. 3. Histological cross-sections of subcutaneous tissue around the implanted site of gelatin–β-TCP sponges incorporating BMP-2 4 weeks after implantation into the back subcutis of rats. The β-TCP contents of gelatin sponges are 0 (a), 25 (b), 50 (c), 75 (d), and 90 wt% (e). Bars correspond to 1 mm.

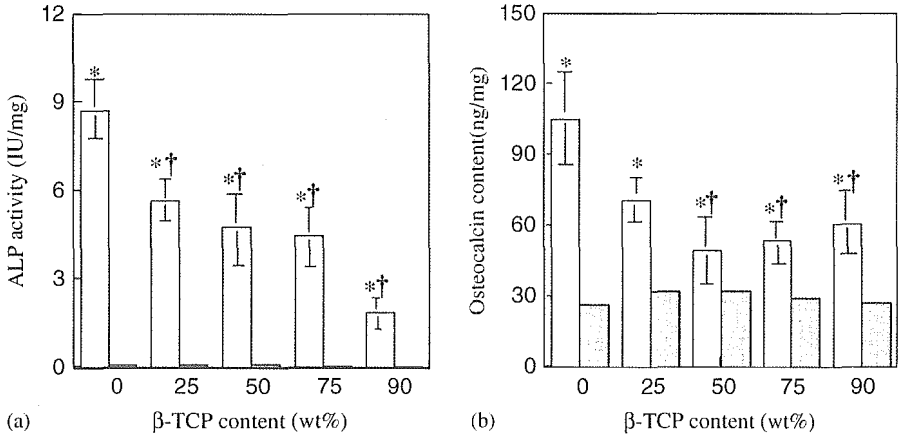

Fig. 4. ALP activity (a) and osteocalcin contents (b) of tissues around the implanted site of gelatin–β-TCP sponges incorporating BMP-2 2 and 4 weeks after implantation, respectively. The BMP-2 doses are 0 (▨) and 5 μg (□). *$p<0.05$, significant against the ALP activity and the osteocalcin contents of tissues around the implanted site of empty gelatin–β-TCP sponges at the corresponding β-TCP amount. †$p<0.05$, significant against the ALP activity and the osteocalcin contents of tissues around the implanted site of the gelatin sponges without β-TCP incorporation.

However, generally a porous structure weakens the mechanical strength of scaffold. Therefore, often the compression modulus of sponge scaffold is not strong enough for cell scaffold application. In experimental and clinical cases, porous HAp and β-TCP have been widely used because of their inherent osteoconductivity [13–22]. However, there are some disadvantages to be improved, such as poor biodegradability and brittle nature. In addition, it is difficult to freely change the shape of bioceramics upon applying to the body site of different shapes during the operation. This study clearly indicates that combination of bioceramics with gelatin is one of the effective strategies to overcome the material problems. The gelatin–β-TCP sponge can be readily cut by a scalpel for the shape change.

When incorporated into gelatin and gelatin–β-TCP sponges and implanted subcutaneously, BMP-2 was retained in the sponges in vivo for more than 1 month and long-termed BMP-2 release was achieved (Fig. 2). No dependence of in vivo BMP-2 release profile on the β-TCP content was observed. This can be explained in terms of the sponge property for growth factor release.

Our previous study demonstrates that a biodegradable hydrogel of the same gelatin enabled BMP-2 to release at the implanted site for extended time periods and the BMP-2 release was governed by the degradation of carrier hydrogel [7]. On the other hand, β-TCP has been investigated as a carrier material for BMP-2 release [44] to show the in vivo release profile similar to that of the gelatin sponge without β-TCP incorporation (data not shown). It is highly conceivable that the BMP-2 adsorbed on the surface of β-TCP can be released through the detachment accompanied with the pore surface erosion, since β-TCP is biodegradable [45]. Taken together, we can say with fair certainty that BMP-2 is released from the gelatin–β-TCP sponge based on the in vivo degradation of both gelatin and β-TCP, although the contribution percentage to the binding site of BMP-2 for release between the gelatin and β-TCP is not clear yet.

The histological study clearly reveals that gelatin and gelatin–β-TCP sponges incorporating BMP-2 induced bone formation homogeneously throughout the sponges (Fig. 3). For the scaffold of hydrogel type, it was difficult to allow cells to infiltrate into the interior of gelatin hydrogels, and consequently osteogenic differentiation induced by the gelatin hydrogel incorporating BMP-2 was observed only around the hydrogel [46], which is quite different from the case of gelatin sponge reported here. As Wozney and Rosen [47] report, the ectopic placement of implants incorporating BMP permits clear differentiation of osteoblast cells throughout osteoinduction for bone tissue formation. It has been considered that BMP activates a set of cellular events including chemotaxis of uncommitted mesenchymal cells and possibly other target cells into the implanted site as well as their differentiation into mineral-depositing osteoblasts. It is likely that the mesenchymal cells recruited into gelatin–β-TCP sponges are stimulated by BMP-2 released from the sponge enough to allow them to differentiate into bone-forming cells like osteoblasts, resulting in efficient induction of bone formation thereat. The extent of bone formed was greater for the gelatin sponge incorporating BMP-2 than that of gelatin–β-TCP sponge incorporating BMP-2. This suggests that the β-TCP presence is not always necessary for bone formation, but the BMP-2 release plays a major role in facilitating osteoinduction activity of gelatin–β-TCP sponge incorporating BMP-2. In addition, it is possible that the bone formation inside the sponge is basically caused by the pore structure.

The ALP activity and osteocalcin content of subcutaneous tissues around the implanted site of gelatin and gelatin–β-TCP sponges incorporating BMP-2 were the highest for the gelatin sponge without β-TCP incorporation (Figs. 4a and b). Since osteoinductive materials allow mesenchymal cells around the implanted site to infiltrate into their pores and to differentiate into osteogenic cells therein [11,12,44], it is conceivable that the osteoinduction activity of the BMP-2-incorporated sponges is influenced both by the in vivo deformation resistance of the sponges and the in vivo profile of BMP-2 release. The difference in the sponge deformation can be explained from the viewpoint of the mechanical stability of sponges rather than the material degradation. When the compression modulus of gelatin–β-TCP sponges was measured in a freeze-dry state, it became higher with the increased amount of β-TCP incorporated. On the other hand, the morphological change of gelatin sponges with or without β-TCP incorporation was evaluated before and after their immersion in collagenase solution (Fig. 5). Although the compression modulus of sponges freeze-dried increased with the increased β-TCP content (Table 1), in a wet state the gelatin–β-TCP sponge collapsed easier than the gelatin sponge without β-TCP incorporation. It is apparent in Fig. 1 that β-TCP granules are dispersed in the matrix of gelatin. It is conceivable that gelatin serves as a binder material between β-TCP particles incorporated to keep the structure of gelatin–β-TCP sponges. Thus, the content of gelatin decreases with an increase in that of β-TCP. As a result, it is likely that the sponges with higher β-TCP contents are collapsed and deformed easily under wet and proteolytic conditions due to faster loss of gelatin mass by degradation. It is possible that this sponge deformation bring about loss of the intrasponge space necessary for bone ingrowth, resulting in reduced osteoinduction activity inside the sponge. On the other hand, we have demonstrated that the in vivo retention of BMP-2 greatly affects the osteoinduction activity of gelatin hydrogels incorporating BMP-2 [7]. In addition, Kaito et al. have demonstrated that even if an interconnected-porous HAp functions as a bioactive and osteoconductive scaffold for bone ingrowth [11,12], the osteoinductivity of a BMP-2/synthetic biodegradable polymer/HAp composite at an ectopic site is affected by the release profile of BMP-2 from the composite [35]. It is conceivable that the osteoinductivity of BMP-2 released plays a major role in inducing ectopic bone formation much more efficiently than the inherent osteoconductivity of HAp. However, in this study, in vivo retention of BMP-2 was not changed by the content of β-TCP incorporation (Fig. 2). Taken together, it is likely that the in vivo deformation of sponges was one factor contributing to the osteoinduction extent of BMP-2-incorporated sponges, although the bioactivity remaining for BMP-2 released and the osteoconductivity are not compared quantitatively among different sponges.

There have been many reports on the polymer/bioceramics composites, such as collagen/HAp, collagen/HAp/polylactide, chitosan/gelatin/TCP, collagen/TCP, and gelatin/TCP, for the scaffold of bone tissue

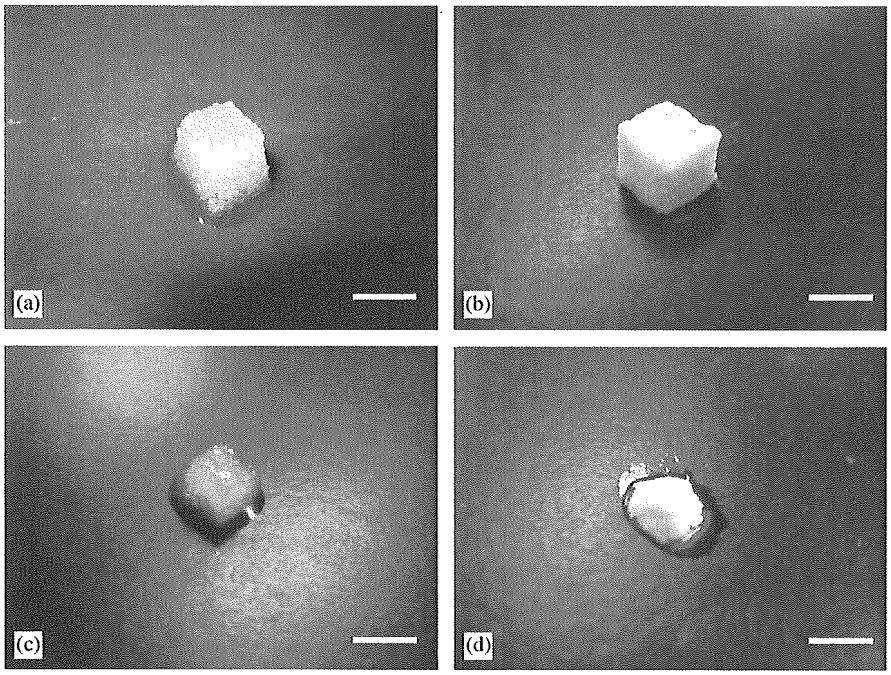

Fig. 5. Appearance of gelatin–β-TCP sponges before (a, b) and after (c, d) in vitro enzymatic degradation. The β-TCP contents of gelatin sponges are 0 (a, c) and 90 wt% (b, d). Bars correspond to 5 mm.

engineering. Most of the reports demonstrate the osteoconductivity of the composites from the in vitro osteogenic culture and the animal experiment of bone defects [23–28]. On the other hand, some research groups have investigated the osteoinduction of BMP-incorporating composites for different animal models [29–35]. However, little has been investigated about the effect of the bioceramic content on the osteoinduction activity. Various methods have been developed to fabricate polymer/bioceramics composites, such as co-precipitation of HAp and collagen in an aqueous collagen solution, HAp deposition onto the pore surface of a collagen sponge, and simple mixing HAp particles with a polymer solution. Since the characteristics of the composites greatly depend on the fabrication methods, it is difficult to directly compare the present data from the results reported. For example, Kaito et al. [35] fabricated the lactide-*co*-ethylene glycol copolymer/HAp composite incorporating BMP by simple coating of BMP/polymer mixture onto the porous HAp block. Asahina et al. [30] implanted HAp granules or block with BMP/collagen mixture into a mandible bone defect of monkey. In these studies, the HAp scaffold can keep the porous structure for bone formation, while the mixture of BMP and polymer enhances bone formation in the scaffold. On the other hand, Hu et al. [32,33] reported BMP-incorporated polylactide scaffold containing the precipitate of collagen and HAp. It is possible that polylactide functions as a binder material to keep the composite structure. Since the degradation of polylactide is much slower than that of gelatin, it is conceivable that the HAp composite with polylactide binder seems to be more stable than that with gelatin binder. The in vivo stability of the sponges used in this study depends on the gelatin mass of binder, while the binder mass decreased with an increased in the β-TCP content. Taken together, it is possible that the pore structure of sponges with the higher β-TCP contents does not maintain due to the faster loss of gelatin mass, resulting in a reduction of the intrasponge space necessary for osteoinduction in gelatin–β-TCP sponges.

Simple foaming of gelatin solution enabled us to prepare the gelatin scaffold of sponge structure not only to induce in vivo infiltration of cells from the surrounding tissues, but also to facilitate in vitro cell seeding. We have demonstrated that the attachment, proliferation, and osteogenic differentiation of mesenchymal stem cells (MSCs) were influenced by the sponge composition of gelatin and β-TCP as the cell scaffold [48]. The balance between the cell density of sponge and the bioactivity of β-TCP may contribute to the extent of MSC differentiation in the sponge. Indeed, the osteoinductive activity without cell seeding decreases with the increased β-TCP content. However, combination of cell seeding technique and the delivery system of osteoinductive growth factor could mimic naturally occurring bone matrix system which provides a favorable environment for osteoinduction, resulting in facilitating in vivo osteoinduction for bone regeneration.

5. Conclusion

Gelatin sponges incorporating various amounts of β-TCP with an average pore size of 180–200 μm were fabricated. The extent of the in vivo BMP-2 remaining was similar for gelatin sponges with different β-TCP contents, although the osteoinduction of gelatin–β-TCP sponges incorporating BMP-2 was affected by the β-TCP content. Since the gelatin–β-TCP sponge collapsed easier than the gelatin sponge without β-TCP incorporation under a proteolytic condition, the maintenance of the intrasponge space necessary for the osteoinduction is one factor contributing to the osteoinduction extent of BMP-2-incorporating sponges. The present findings will give fundamental information to design the osteoinductive scaffold for bone tissue engineering in terms of bone cell scaffold and growth factor delivery system.

Acknowledgement

We thank Dr. Takayoshi Nakano and Dr. Koji Hagihara of Department of Material Science and Engineering, Graduate School of Engineering, Osaka University, for instruction of EDX analysis.

References

[1] Langer R, Vacanti JP. Tissue engineering. Science 1993;260:920–6.
[2] Petite H, Viateau V, Bensaid W, Meunier A, de Pollak C, Bourguignon M, Oudina K, Sedel L, Guillemin G. Tissue-engineered bone regeneration. Nat Biotechnol 2000;18:959–63.
[3] Lieberman JR, Daluiski A, Einhorn TA. The role of growth factors in the repair of bone. Biology and clinical applications. J Bone Jt Surg 2002;84-A:1032–44.
[4] Reddi AH. Bone morphogenetic proteins: from basic science to clinical applications. J Bone Jt Surg 2001;83-A(Suppl. 1, Part 1):S1–6.
[5] Gittens SA, Uludag H. Growth factor delivery for bone tissue engineering. J Drug Target 2001;9:407–29.
[6] Zekorn D. Intravascular retention, dispersal, excretion and breakdown of gelatin plasma substitutes. Bibl Haematol 1969;33: 131–40.
[7] Yamamoto M, Takahashi Y, Tabata Y. Controlled release by biodegradable hydrogels enhances the ectopic bone formation of bone morphogenetic protein. Biomaterials 2003;24:4375–83.
[8] Bordenave L, Caix J, Basse-Cathalinat B, Baquey C, Midy D, Baste JC, Constans H. Experimental evaluation of a gelatin-coated polyester graft used as an arterial substitute. Biomaterials 1989;10:235–42.
[9] Warocquier-Clerout R, Lee YS, Penhoat J, Sigot-Luizard MF. Comparative behaviour of L-929 fibroblastic and human endothelial cells onto crosslinked protein substrates. Cytotechnology 1990;3:259–69.
[10] Ma Z, Gao C, Gong Y, Ji J, Shen J. Immobilization of natural macromolecules on poly-L-lactic acid membrane surface in order to improve its cytocompatibility. J Biomed Mater Res 2002;63:838–47.
[11] Damien CJ, Parsons JR. Bone graft and bone graft substitutes: a review of current technology and applications. J Appl Biomater 1991;2:187–208.
[12] Bauer TW, Simth ST. Bioactive materials in orthopaedic surgery: overview and regulatory considerations. Clin Orthop Relat Res 2002;395:11–22.
[13] Yang Z, Yuan H, Tong W, Zou P, Chen W, Zhang X. Osteogenesis in extraskeletally implanted porous calcium phosphate ceramics: variability among different kinds of animals. Biomaterials 1996;17:2131–7.
[14] Knabe C, Driessens FC, Planell JA, Gildenhaar R, Berger G, Reif D, Fitzner R, Radlanski RJ, Gross U. Evaluation of calcium phosphates and experimental calcium phosphate bone cements using osteogenic cultures. J Biomed Mater Res 2000;52: 498–508.
[15] Yuan H, Li Y, de Bruijn JD, de Groot K, Zhang X. Tissue responses of calcium phosphate cement: a study in dogs. Biomaterials 2000;21:1283–90.
[16] Mankani MH, Kuznetsov SA, Fowler B, Kingman A, Robey PG. In vivo bone formation by human bone marrow stromal cells: effect of carrier particle size and shape. Biotechnol Bioeng 2001;72:96–107.
[17] Erbe EM, Marx JG, Clineff TD, Bellincampi LD. Potential of an ultraporous beta-tricalcium phosphate synthetic cancellous bone void filler and bone marrow aspirate composite graft. Eur Spine J 2001;10(Suppl. 2):S141–6.
[18] Livingston T, Ducheyne P, Garino J. In vivo evaluation of a bioactive scaffold for bone tissue engineering. J Biomed Mater Res 2002;62:1–13.
[19] Boo JS, Yamada Y, Okazaki Y, Hibino Y, Okada K, Hata K, Yoshikawa T, Sugiura Y, Ueda M. Tissue-engineered bone using mesenchymal stem cells and a biodegradable scaffold. J Craniofac Surg 2002;13:231–9.
[20] Kasten P, Luginbuhl R, van Griensven M, Barkhausen T, Krettek C, Bohner M, Bosch U. Comparison of human bone marrow stromal cells seeded on calcium-deficient hydroxyapatite, beta-tricalcium phosphate and demineralized bone matrix. Biomaterials 2003;24:2593–603.
[21] Shimaoka H, Dohi Y, Ohgushi H, Ikeuchi M, Okamoto M, Kudo A, Kirita T, Yonemasu K. Recombinant growth/differentiation factor-5 (GDF-5) stimulates osteogenic differentiation of marrow mesenchymal stem cells in porous hydroxyapatite ceramic. J Biomed Mater Res 2004;68A:168–76.
[22] Ruhe PQ, Kroese-Deutman HC, Wolke JG, Spauwen PH, Jansen JA. Bone inductive properties of rhBMP-2 loaded porous calcium phosphate cement implants in cranial defects in rabbits. Biomaterials 2004;25:2123–32.
[23] Ignatius AA, Ohnmacht M, Claes LE, Kreidler J, Palm F. A composite polymer/tricalcium phosphate membrane for guided bone regeneration in maxillofacial surgery. J Biomed Mater Res 2001;58:564–9.
[24] Laurencin CT, Attawia MA, Lu LQ, Borden MD, Lu HH, Gorum WJ, Lieberman JR. Poly(lactide-*co*-glycolide)/hydroxyapatite delivery of BMP-2-producing cells: a regional gene therapy approach to bone regeneration. Biomaterials 2001;22:1271–7.
[25] Du C, Cui FZ, Zhu XD, de Groot K. Three-dimensional nano-HAp/collagen matrix loading with osteogenic cells in organ culture. J Biomed Mater Res 1999;44:407–15.
[26] Itoh S, Kikuchi M, Koyama Y, Takakuda K, Shinomiya K, Tanaka J. Development of an artificial vertebral body using a novel biomaterial, hydroxyapatite/collagen composite. Biomaterials 2002;23:3919–26.
[27] Rodrigues CV, Serricella P, Linhares AB, Guerdes RM, Borojevic R, Rossi MA, Duarte ME, Farina M. Characterization of a bovine collagen–hydroxyapatite composite scaffold for bone tissue engineering. Biomaterials 2003;24:4987–97.

[28] Lickorish D, Ramshaw JA, Werkmeister JA, Glattauer V, Howlett CR. Collagen–hydroxyapatite composite prepared by biomimetic process. J Biomed Mater Res 2004;68A:19–27.
[29] Kamegai A, Shimamura N, Naitou K, Nagahara K, Kanematsu N, Mori M. Bone formation under the influence of bone morphogenetic protein/self-setting apatite cement composite as a delivery system. Biomed Mater Eng 1994;4:291–307.
[30] Asahina I, Watanabe M, Sakurai N, Mori M, Enomoto S. Repair of bone defect in primate mandible using a bone morphogenetic protein (BMP)–hydroxyapatite–collagen composite. J Med Dent Sci 1997;44:63–70.
[31] Tuominen T, Jamsa T, Oksanen J, Tuukkanen J, Gao TJ, Lindholm TS, Jalovaara P. Composite implant composed of hydroxyapatite and bone morphogenetic protein in the healing of a canine ulnar defect. Ann Chir Gynaecol 2001;90:32–6.
[32] Hu Y, Zhang C, Zhang S, Xiong Z, Xu J. Development of a porous poly(L-lactic acid)/hydroxyapatite/collagen scaffold as a BMP delivery system and its use in healing canine segmental bone defect. J Biomed Mater Res 2003;67A:591–8.
[33] Hu YY, Zhang C, Lu R, Xu JQ, Li D. Repair of radius defect with bone-morphogenetic-protein loaded hydroxyapatite/collagen–poly(L-lactic acid) composite. Chin J Traumatol 2003;6:67–74.
[34] Liao SS, Guan K, Cui FZ, Shi SS, Sun TS. Lumbar spinal fusion with a mineralized collagen matrix and rhBMP-2 in a rabbit model. Spine 2003;28:1954–60.
[35] Kaito T, Myoui A, Takaoka K, Saito N, Nishikawa M, Tamai N, Ohgushi H, Yoshikawa H. Potentiation of the activity of bone morphogenetic protein-2 in bone regeneration by a PLA-PEG/hydroxyapatite composite. Biomaterials 2005;26:73–9.
[36] Matsuda K, Suzuki S, Isshiki N, Yoshioka K, Okada T, Ikada Y. Influence of glycosaminoglycans on the collagen sponge component of a bilayer artificial skin. Biomaterials 1990;11:351–5.
[37] Chen G, Ushida T, Tateishi T. A biodegradable hybrid sponge nested with collagen microsponges. J Biomed Mater Res 2000;51:273–9.
[38] Greenwood FC, Hunter WM, Gglover TC. The preparation of ^{131}I-labeled human growth hormone of high specific radioactivity. Biochem J 1963;89:114–23.
[39] Kobayashi D, Takita H, Mizuno M, Totsuka Y, Kuboki Y. Time-dependent expression of bone sialoprotein fragments in osteogenesis induced by bone morphogenetic protein. J Biochem 1996;119:475–81.
[40] Tabata Y. Tissue regeneration based on growth factor release. Tissue Eng 2003;9(Suppl. 1):S5–15.
[41] Kawai K, Suzuki S, Tabata Y, Ikada Y, Nishimura Y. Accelerated tissue regeneration through incorporation of basic fibroblast growth factor-impregnated gelatin microspheres into artificial dermis. Biomaterials 2000;21:489–99.
[42] Klawitter JJ, Hulbert SF. Application of porous ceramics for the attachment of load bearing internal orthopedic applications. J Biomed Mater Res Symp 1971;2:161–229.
[43] Robinson BP, Hollinger JO, Szachowicz EH, Brekke J. Calvarial bone repair with porous D,L-polylactide. Otolaryngol Head Neck Surg 1995;112:707–13.
[44] Urist MR, Lietze A, Dawson E. β-Tricalcium phosphate delivery system for bone morphogenetic protein. Clin Orthop Relat Res 1984;187:277–80.
[45] Klein CPAT, Driessen AA, de Groot K, van den Hooff A. Biodegradation behavior of various calcium phosphate materials in bone tissue. J Biomed Mater Res 1983;17:769–84.
[46] Yamamoto M, Kato K, Ikada Y. Effect of the structure of bone mophogenetic protein carriers on ectopic bone regeneration. Tissue Eng 1996;2:315–26.
[47] Wozney JM, Rosen V. Bone morphogenetic protein and bone morphogenetic protein gene family in bone formation and repair. Clin Orthop Relat Res 1998;346:26–37.
[48] Takahashi Y, Yamamoto M, Tabata Y. Osteogenic differentiation of mesenchymal stem cells in biodegradable sponges composed of gelatin and β-tricalcium phosphate. Biomaterials 2005 in press.

Available online at www.sciencedirect.com
SCIENCE DIRECT®
ELSEVIER
Colloids and Surfaces A: Physicochem. Eng. Aspects xxx (2006) xxx–xxx
COLLOIDS AND SURFACES A
www.elsevier.com/locate/colsurfa

Control of hepatocyte adhesion and function on self-organized honeycomb-patterned polymer film

Masaru Tanaka[a,b,*], Kazutaka Nishikawa[c], Hisashi Okubo[d], Hirofumi Kamachi[d], Tomoaki Kawai[d], Michiaki Matsushita[b,d], Satoru Todo[b,d], Masatsugu Shimomura[b,e]

[a] *Creative Research Initiative "Sousei" (CRIS), Hokkaido University, Kita-Ku N21W10, Sapporo 001-0021, Japan*
[b] *CREST, Japan Science and Technology Corporation (JST), Honchou 4-1-8, Kawaguchi 332-0012, Japan*
[c] *Graduate School of Science, Hokkaido University, Kita-Ku N11W6, Sapporo 001-0021, Japan*
[d] *Graduate School of Medicine, Hokkaido University, Kita-Ku N15W7, Sapporo 060-8638, Japan*
[e] *Nanotechnology Research Center, Research Institute for Electronic Science, Hokkaido University, Kita-Ku N21W10, Sapporo 001-0021, Japan*

Received 31 July 2005; received in revised form 26 November 2005; accepted 29 November 2005

Abstract

Hepatocytes were cultured on a honeycomb-patterned polymer film (honeycomb film) formed by self-organization in order to investigate the influence of the honeycomb pattern on cell behavior. The changes in cell morphologies and actin filaments were observed by optical, fluorescence, and scanning electron microscopy. Hepatocytes were flattened, and the actin filaments appeared conspicuously in the spreading regions on a flat film. In contrast, the hepatocytes that were cultured on the honeycomb film were observed to form a spherical shape, and the actin filaments were localized inside the edge of the spheroid. The spheroids were observed within several hours after seeding on the honeycomb film; they were attached and the spheroid shape was maintained without any deformation. The spheroids expressed a higher level of liver specific function than the cell monolayers on the flat film. These results suggest that the honeycomb film is a suitable material for tissue engineering scaffolds and biomedical devices.

Keywords: Cell adhesion; Hepatocyte; Self-organization; Hepatic function; Cell surface interaction

1. Introduction

The design of nano- and microstructures by self-organization is one of the most important issues for creating new materials. This design has a variety of potential applications in tissue engineering scaffolds. The scaffolds must provide suitable substrates for cell adhesion, proliferation, and differentiated function [1–4]. Porous polymer materials have been investigated and are widely used in biomedical applications such as tissue engineering and artificial organs. These porous materials have been fabricated by many methods [5–14], including lithography, micro-contact printing, phase separation, solution casting/salt leaching, freeze-immersion, emulsion freeze-drying, gel casting, gas forming, and colloidal assemblies as templates. These techniques are certainly useful in the fabrication of the porous materials. However, these techniques require a large amount of energy and involve many processes. In addition, there is a limited variety of materials available for scaffolds. The preparation of honeycomb films by casting a polymer solution on solid substrates has been previously reported [15–23]. This method has a great advantage in that the films can be prepared with ease, at a low cost, and with less limitation of materials for scaffolds.

One of the key issues in liver tissue engineering and the development of bioartificial liver assist devices is the design of an effective porous polymer scaffold for hepatocyte adhesion and hepatic function. However, it is difficult to control hepatocyte adhesion and enhance the hepatic function in vitro, and the hepatocyte activities are often limited by the lack of the liver specificity of the environment. In this study, we describe the fabrication of highly regular porous surfaces (honeycomb films) formed by a solution casting technique under humid air condi-

* Corresponding author.
E-mail address: tanaka@poly.es.hokudai.ac.jp (M. Tanaka).

0927-7757/$ – see front matter © 2005 Elsevier B.V. All rights reserved.
doi:10.1016/j.colsurfa.2005.11.098

tion, and the culture of hepatocytes on these films in order to investigate cell adhesion and function.

2. Experimental

2.1. Materials

A copolymer of dodecylacrylamide and ω-carboxyhexylacrylamide as shown in Fig. 1a was used as an emulsifier in this study. The copolymer was synthesized by the previously reported method [24]. The copolymer is amphiphilic because the polymer forms a stable monolayer at the air–water interface. The copolymer is abbreviated as Cap in this study. The molecular weight of the polymer, which was estimated by size exclusion chromatography, is 4.5×10^4 g/mol. The water was purified by a Millipore system (Milli-Q, Millipore). Organic solvents and other chemicals were commercially available and were used without further purification.

2.2. Preparation of honeycomb and flat films

The honeycomb film was prepared on a glass substrate by the method described previously [15–23]. Briefly, Cap was dissolved in chloroform at a concentration of 5 g/L. The polymer solution was poured into a round glass dish (9.3 cm in diameter) under blowing highly humid air (1.0 L/min). The Cap flat film was prepared as follows. The Cap solution (5 g/L) was dropped onto a slide glass. The cover glass with the polymer layer was spun at 1000 rpm for 30 s by using a spin coater (1H-7D, Mikasa).

2.3. Hepatocyte cell culture

Using a modified two-step collagenase perfusion technique in situ, hepatocytes were isolated from 6- to 7-week-old male Wistar rats weighing 200–300 g [25]. The obtained cells were washed four times by centrifugation at $50 \times g$ for 1 min. The hepatocyte viability was determined by trypan blue exclusion. The hepatocytes were cultivated in serum-free Williams' E medium supplemented with 0.1 μM $CuSO_4 \cdot 5H_2O$ (Wako Pure Chemical Industries Ltd., Osaka, Japan), 25 nM Na_2SeO_3 (Wako), 1.0 μM $ZnSO_4 \cdot 7H_2O$ (Wako), 0.1 μM insulin (Sigma Chemicals Co., St. Louis, MO), 1.0 μM dexamethasone (Sigma), 20 ng/mL epidermal growth factor (Sigma), 100 μg/mL ascorbic acid diphosphate (Sigma), 5 KIE/mL aprotinin (Bayer, Germany), 48 μg/mL gentamicin (Schering-Plough, USA), and 100 ng/mL chloramphenicol (Sankyo, Japan). The cell suspension of the hepatocytes was adjusted to the cell density of 2.0×10^5 cells/well (24-well plates) in Williams' E medium. The hepatocytes were seeded onto polymer substrates that were immersed in the medium for over 6 h. They were then incubated at 37 °C in 95% air containing 5% CO_2. The culture medium exchange was carried out every 24 h. The morphologies of hepatocytes after seeding were observed using a phase contrast microscope (IX 70, Olympus).

2.4. Scanning electron microscopic observation

The cells that were cultured 72 h after seeding were fixed in 2% glutaraldehyde in phosphate-buffered saline (PBS) (Wako) overnight at 4 °C. After washing three times with PBS, each sample was fixed in 1.0% osmium tetroxide (Wako) aqueous solution for 1 h and was rinsed in PBS. Subsequently, the samples were dehydrated by washing in increasing ethanol concentrations and then air-dried. The samples were transferred to microporous specimen capsules and dried by means of a critical point dryer (HCP-2, Hitachi Co., Tokyo, Japan). The dried samples were mounted on aluminum stages by double stick tape and coated with palladium gold (approximately 5 nm of coating) by using an ion sputter coater (E-1030, Hitachi). All samples were observed using a scanning electron microscope (SEM) (S-3500N, Hitachi).

2.5. Actin staining and confocal laser scanning microscopy

The actin filaments in the hepatocytes that were cultured 72 h after seeding were stained. After washing with PBS, the cells were fixed with 3.7% formaldehyde for 30 min at room temperature. The cells were washed twice with PBS and permeabilized for 15 min with 0.1% Triton X-100 (Sigma) and 1.0% bovine serum albumin (Sigma) in PBS. After rinsing twice with PBS, the cells were stained for 30 min with rhodamine-phalloidin (Molecular Probes, Eugene, OR) in PBS at room temperature. The stained cells were then rinsed four times with PBS and immersed for 1 h at the fourth rinse. All samples were removed to slides. Coverslips were applied onto the samples and sealed with manicure. The confocal laser scanning microscope (CLSM) (MRC-1024, Bio-Rad Laboratories Inc., Hercules, CA) was utilized for observation. The Zeiss Plan-Neofluar 40×/0.75 NA objective lens was used to visualize the actin filaments. The

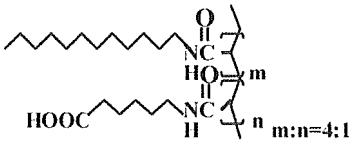

(a) **Amphiphilic polymer (Cap)**

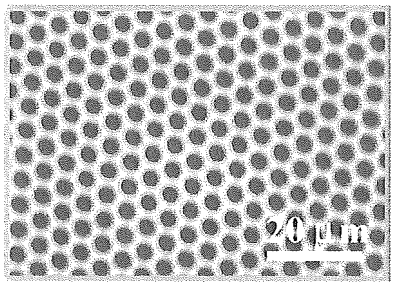

(b)

Fig. 1. Chemical structure of a copolymer of dodecylacrylamide and ω-carboxyhexylacrylamide (Cap) and SEM image of a honeycomb film.

excitation wavelength was set to 568 nm, and a 585 nm long-pass filter was utilized to collect the emitted light. Images were acquired using LaserSharp software (version 3.2, Bio-Rad Laboratories Inc.).

2.6. Urea synthesis

Urea concentration was measured by the diacetyl monoxime method [26]. The culture medium was replaced with Williams' E medium containing 5 mM NH_4Cl, and the hepatocytes were cultivated in this medium with ammonia for 2 h. The samples cultivated in this medium were removed from the well and stored separately at −40 °C.

2.7. DNA content

To assess the number of hepatocytes, the DNA contents of the cultured hepatocytes were measured by 4′, 6-diamidino-2-phenylindole (DAPI) fluorometry using calf thymus DNA as a standard [27]. The cells were detached from the dish by adding protease and incubating them at 37 °C for 1 h. The cell pellets were suspended in a solution containing 50 mM Tris–Cl, 0.1 M NaCl, and 5 mM edetic acid and then homogenized using an ultrasonic homogenizer (Branson Sonifier 250, Branson Sonic Power Co., Danbury, CT). Following the addition of 100 ng/mL DAPI, the fluorescence of the solution was measured with a spectrofluorophotometer (RF-510; Shimadzu, Kyoto, Japan). All samples of the DNA were stored at −40 °C. The data on the measurement of urea and DNA concentration were expressed as mean ± SD, and statistical analysis was performed using ANOVA. A P value of less than 0.05 was considered statistically significant.

3. Results and discussion

3.1. Honeycomb film

The honeycomb-patterned surface showed a highly regular hexagonal arrangement of holes with a pore size of 5 μm (Fig. 1b). The condensation of water from the air occurred due to evaporation cooling when a water-immiscible solvent was used. The self-packed and monodispersed water droplets formed on the solution surface acted as a temporary template of the pores. In general, the condensed water droplets are not stable and eventually start coalescing. In order to prepare the highly regular porous (honeycomb-patterned) film, the stabilization of the water droplets is necessary. The role of the amphiphilic polymer in the pattern formation is to prevent the fusion of the water droplets. Cap (Fig. 1a) as a surfactant contributes to stabilized the water droplets at the polymer solution and water interface. As a result, the water droplets are prevented from fusing to each other by the intervening the amphiphilic polymer layer. Most of polymers dissolved in water-immiscible solvent can be fabricated to the (honeycomb-patterned film by the addition of Cap. Various experimental factors affect the pore structures. The pore size can be controlled in the range of 100 nm to 50 μm by changing the casting conditions [15–23]. Unlike other template or lithographic methods, the advantage of this method is the ease with which such patterned surfaces can be created using various materials without large energy consumption.

3.2. Morphologies of adhered hepatocytes on honeycomb and flat films

Most tissue-derived cells are anchorage dependent and require attachment to a solid surface for viability and growth. Therefore, the initial events that occur when a cell approaches a surface are of fundamental interest. In tissue engineering, cell adhesion to a surface is critical because adhesion precedes other events, such as cell spreading, cell migration, and differentiated cell functions.

The viability of hepatocytes prepared from rat liver was 90–95%. Fig. 2 shows the time course of the morphologies of adhered hepatocytes on both flat and honeycomb films observed using a phase contrast microscope. Seventy-two hours after culture, the morphologies of adhered hepatocytes on both films were observed using SEM (Fig. 3). The morphology of hepatocytes on the honeycomb film was compared with that of hepatocytes on the flat film. The morphologies of hepatocytes on both films were observed to be different. On the flat film, the hepatocytes appeared to have a typical monolayer morphology (Fig. 2a). The hepatocytes on the flat film had already attached themselves to the film surface at 6 h, and cell spreading and nuclei were observed subsequently. The attached hepatocytes were observed to form a spreading morphology known as monolayer at 24 h. This monolayer had extended sufficiently at 72 h (Figs. 2a and 3a). The flat film possesses an adhesive property because the monolayer appears on a substrate that has this property, such as tissue culture polystyrene dish or collagen coated dish.

Another typical morphology of hepatocyte spheroids was observed on the honeycomb film (Figs. 2b and 3b). Although the hepatocytes on the honeycomb film had already attached themselves to the film surface in a manner identical to those on a flat film at 6 h, cell spreading and flattening of the nuclei were rarely demonstrated. The honeycomb film restricted cell spreading, but did not inhibit cell adhesion. The attached hepatocytes were gathered gradually. The spheroids then outgrew gradually in the culture, and an increase in the mean size of the spheroids was observed with time (0–12 h). Rapid spheroid formation became possible, and the spheroids could be fixed on the honeycomb film. The size of the spheroids was maintained after 24 h at approximately 100 μm, and deformation and detachment of the spheroids from the honeycomb film were not observed. This behavior is expected to exhibit better and longer hepatic function. It should be noted that both the flat and honeycomb films were prepared from the same polymer. This implies that the topological property of the honeycomb film affected the formation of hepatocyte morphology. The honeycomb film may be appropriate for the regulation of the degree of cell–cell versus cell–material interactions, and the honeycomb pattern variations can also affect liver specific functions.

The mechanism of the interaction between the hepatocytes and the honeycomb film require further investigation. However,

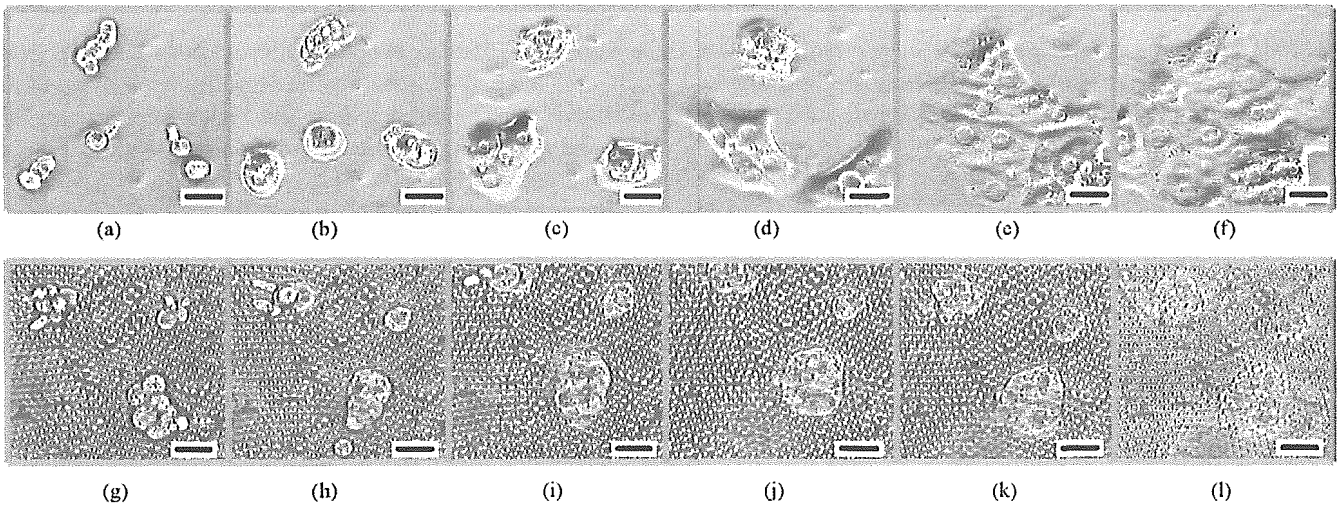

Fig. 2. Time course of the morphologies of hepatocytes in phase contrast images on flat film at (a) 6 h, (b)12 h, (c) 24 h, (d) 36 h, (e) 48 h, and (f) 72 h; and on honeycomb film at (g) 6 h, (h) 12 h, (i) 24 h, (j) 36 h, (k) 48 h, and (l) 72 h after culture. These images were obtained from the same view field (bar: 50 μm).

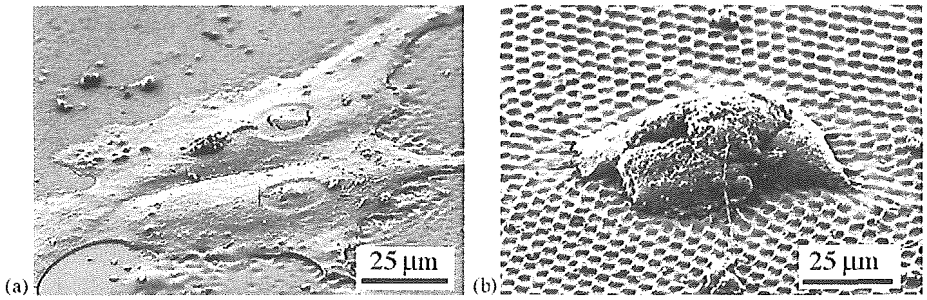

Fig. 3. SEM images of hepatocytes 72 h after culture on (a) flat film and (b) honeycomb film.

the strategy of immobilization and stabilization of hepatocyte sheroids through the use of honeycomb films would prove advantageous in the design of a bioartificial liver assist device, where the hepatocytes could attach themselves to a film with a high surface area, maintain their functions, and remain stable against the perfusion and shear forces in the bioreactor.

3.3. Actin filaments

Cytoskeletal actin is known as a liner protein that forms the shape of cells. In addition, it is important even in functional expressions such as proliferation and migration. These events involve the development of specific intercellular adhesions and redistribution of cell–cell and cell–material adhesion forces, which are intimately related to the dynamic cytoskeletal organization.

Fig. 4 shows CLSM images of actin filaments in adhered hepatocytes on both flat and honeycomb films. The actin filaments appeared conspicuously in the spreading regions of the hepatocytes on the flat film (Fig. 4a). Although the actin filaments in the cytoplasm could not be seen at 24 h, they were observed in great amounts of fibrous actin at 72 h (Fig. 4a), while the actin filaments existed locally in the intracellular edge with the forming morphology in which the cells overlapped the

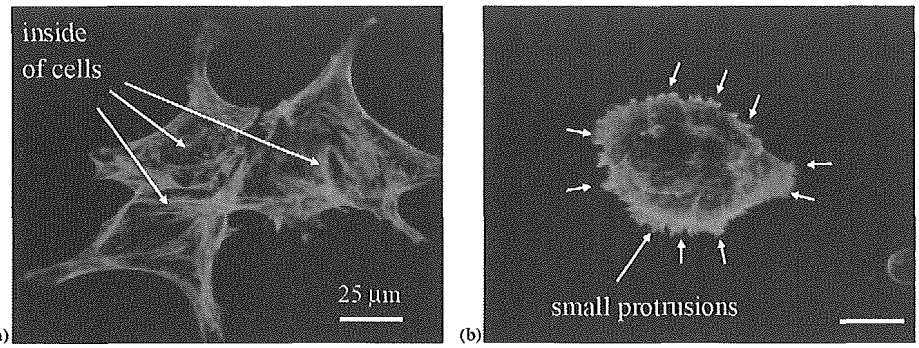

Fig. 4. CLSM images of actin localization in adhered hepatocytes at 72 h after culture on (a) flat film and (b) honeycomb film.

spheroids on the honeycomb film (Fig. 4b). Small protrusions were observed around the spheroids, and the actin filament was localized along the protrusions (Fig. 4b). These results indicated that the honeycomb film could control hepatocyte adhesion following cytoskeletal protein production.

The results obtained in this study increase the interest in the Rho family of small GTPase. The Rho family has emerged as the key regulator of the actin cytoskeleton and it coordinates the control of cellular activities, such as gene transcription and adhesion [28]. It is possible that the topological properties of the honeycomb film affected signal transduction with the Rho family, since morphology and actin localization of hepatocytes on the honeycomb film were different from those on the flat film.

3.4. Urea synthesis

The hepatocyte morphology and formation of actin filaments are important factors that affect the hepatocyte function. Spheroidal aggregates of hepatocytes, or hepatocyte spheroids, are known to exhibit better and longer hepatocyte functions than hepatocytes produced by monolayer culture [29], and they are expected to be a promising candidate for the main bioreactor component of hybrid artificial livers. Next, we investigated liver specific functions.

Fig. 5 shows the data on urea synthesis profiles 72 h after culture on both the flat and honeycomb films. The urea level in the hepatocytes cultured on the honeycomb film was higher than that of the hepatocytes cultured on the flat film. As mentioned above, the result indicated that urea synthesis reflected the hepatocyte morphology since it was known that an interaction between morphology and functions results in spheroids with differentiated functions that are higher than those of monolayer hepatocytes. It was considered that hepatocytes on the honeycomb film were formed as tissue-like structures, and the high expression of urea synthesis appeared accordingly. Thus, the enhancement and maintenance of hepatic function for a long period of time may be possible by utilizing the honeycomb film.

We found that the honeycomb-patterned structure quite affected not only cell adhesion but also actin organization and urea synthesis of the hepatocytes. These results indicate that the physical properties of films should be considered in the cases where porous films were used as scaffolds. To date, there is little information on porous-film-induced topological effects on hepatocytes, although an optimal balance between the degree of cell–cell and cell–material interactions has been recognized as a critical factor for guiding three-dimensional cellular organization and improving hepatic function on porous films for tissue engineering scaffolds [10,30].

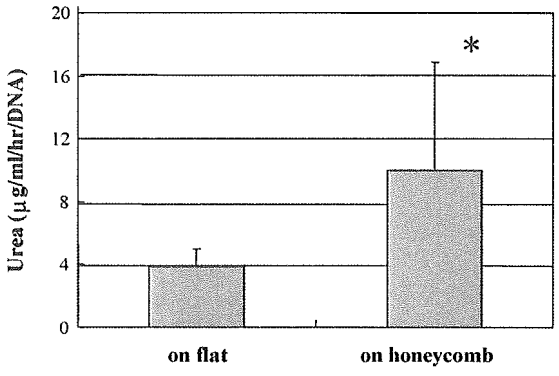

Fig. 5. Urea synthesis of hepatocytes 72 h after culture on flat and honeycomb films. ($^{*}p < 0.05$ vs. flat, mean ± standard deviation, $n = 6$).

The honeycomb film is also a useful tool for obtaining insights into the mechanism of cell–cell and cell–material interactions, which is one of the central research topics in nanobiotechnology. At present, the mechanism by which the cells recognize the honeycomb film in cultures is not clear. It is generally known that adhesion and morphology of cells are influenced by the variety and structure of adsorbed proteins on the material surface [31]. We have reported the adsorbed proteins and water structure on polymer in order to clarify the main factor that causes cell–material and protein–material interactions [32–48]. Future investigation will focus on the factor causing the honeycomb-film-induced changes in the morphologies and functions of hepatocytes in terms of hepatocyte adhesion receptors and focal adhesion that involve hepatocyte intercellular signal transduction and gene expression.

4. Conclusions

Honeycomb films have a strong influence on cell adhesion, actin organization, and hepatic function. The hepatocytes on flat films exhibited greater cell spreading and flattening; however, they did not express appropriate liver specific functions. In contrast, the hepatocytes that were cultured on the honeycomb film formed a spherical shape and enhanced the hepatic function. The fabrication of honeycomb films by self-organization can become an effective method that does not require lithography and large energy consumption. The honeycomb films can be potentially applied in tissue engineering scaffolds and biomedical devices.

Acknowledgements

This study is supported by grants-in-aid from Japan Science and Technology Corporation (JST) and Special Coordination Funds for Promoting Science and Technology.

References

[1] L.G. Cima, J.P. Vacanti, C. Vacanti, J. Biomech. Eng. 113 (1991) 143–151.
[2] L.G. Griffith, B. Wu, M.J. Cima, Ann. N.Y. Acad. Sci. 831 (1997) 382–397.
[3] A.G. Mikos, Y. Bao, L.G. Cima, J. Biomed. Mater. Res. 27 (1993) 183–189.
[4] C.S. Chen, M. Mrksich, S. Huang, G.M. Whitesides, D.E. Ingber, Science 276 (1997) 1425–1427.
[5] P. Clark, S. Britland, P. Connolly, J. Cell Sci. 105 (1993) 203–212.
[6] L. Kam, W. Shain, J.N. Turner, R. Bizios, Biomaterials 22 (2001) 1049–1054.
[7] J. Tan, W.M. Saltzman, Biomaterials 23 (2002) 3215–3225.
[9] J.B. Recknor, J.C. Recknor, D.S. Sakaguchi, S.K. Mallapragada, Biomaterials 25 (2004) 2753–2767.
[10] A.G. Mikos, A.J. Thorsen, L.A. Czerwonka, Y. Bao, R. Langer, D.N. Winslow, J.P. Vacanti, Polymer 35 (1994) 1068–1077.

[11] M.C. Wake, P.K. Gupta, A.G. Mikos, Cell Transplant. 5 (1996) 465–473.
[12] A.T. Gutsche, H. Lo, J. Zurlo, J. Yager, K.W. Leong, Biomaterials 17 (1996) 387–393.
[13] L.D. Harris, B.S. Kim, D.J. Mooney, J. Biomed. Mater. Res. 42 (1998) 396–402.
[14] Y.S. Nam, J.J. Yoon, T.G. Park, J. Biomed. Mater. Res. 53 (2000) 1–7.
[15] N. Maruyama, T. Koito, J. Nishida, T. Sawadaishi, X. Cieren, K. Ijiro, O. Karthaus, M. Shimomura, Thin Solid Films 327–329 (1998) 854–856.
[16] O. Karthaus, N. Maruyama, X. Cieren, M. Shimomura, H. Hasegawa, T. Hashimoto, Langmuir 16 (2000) 6071–6076.
[17] M. Shimomura, T. Sawadaishi, Curr. Opin. Colloid. Interface Sci. 6 (2001) 11–16.
[18] K. Sato, M. Tanaka, K. Hasebe, M. Takebayashi, K. Nishikawa, T. Kawai, M. Matsushita, S. Todo, M. Shimomura, Int. J. Nanosci. 1 (2002) 689–693.
[19] T. Nishikawa, R. Ookura, J. Nishida, K. Arai, J. Hayashi, N. Kurono, T. Sawadaishi, M. Hara, M. Shimomura, Langmuir 18 (2002) 5734–5739.
[20] H. Yabu, M. Tanaka, K. Ijiro, M. Shimomura, Langmuir 19 (2003) 6297–6300.
[21] M. Tanaka, M. Takebayashi, M. Miyama, J. Nishida, M. Shimomura, Bio-med. Mater. Eng. 14 (2004) 439–445.
[22] A. Tsuruma, M. Tanaka, N. Fukushima, M. Shimomura, J. Surf. Sci. Nanotech. 3 (2005) 159–164.
[23] H. Yabu, M. Takebayashi, M. Tanaka, M. Shimomura, Langmuir 21 (2005) 3235–3237.
[24] S. Nishimura, K. Yamada, J. Am. Chem. Soc. 119 (1997) 10555–10556.
[25] P.O. Seglen, Methods Cell Biol. 13 (1976) 29–83.
[26] W.H. Marsh, B. Fingerhut, H. Miller, Clin. Chem. 11 (1965) 624–627.
[27] C.F. Brunk, K.C. Jones, T.W. James, Anal. Biochem. 92 (1979) 497–500.
[28] A. Hall, Science 279 (1998) 509–514.
[29] J. Landry, D. Bernier, C. Ouellet, R. Goyett, N. Marceau, J. Cell Biol. 101 (1985) 914–923.
[30] C.S. Ranucci, A. Kumar, S.P. Batra, P.V. Moghe, Biomaterials 21 (2000) 783–793.
[31] J.D. Andrade, in: J.D. Andrade (Ed.), Surface and Interfacial Aspects of Biomedical Polymers, Plenum Publishers, New York, 1985, p. 1.
[32] M. Tanaka, T. Motomura, M. Kawada, T. Anzai, Y. Kasori, T. Shiroya, K. Shimura, M. Onishi, A. Mochizuki, Biomaterials 21 (2000) 1471–1481.
[33] M. Tanaka, T. Motomura, M. Kawada, T. Anzai, Y. Kasori, T. Shiroya, K. Shimura, M. Onishi, A. Mochizuki, Y. Okahata, Jpn. J. Artif. Organs. 9 (2000) 209–216.
[34] M. Tanaka, T. Motomura, N. Ishii, K. Shimura, M. Onishi, A. Mochizuki, T. Hatakeyama, Polym. Int. 49 (2000) 1709–1713.
[35] H. Kitano, K. Ichikawa, M. Fukuda, A. Mochizuki, M. Tanaka, J. Colloid Surface Sci. 242 (2001) 133–140.
[36] K. Ichikawa, T. Mori, H. Kitano, M. Fukuda, A. Mochizuki, M. Tanaka, J. Polym. Sci., B Polym. Phys. 39 (2001) 2175–2182.
[37] M. Tanaka, A. Mochizuki, T. Motomura, K. Shimura, M. Onishi, Y. Okahata, Colloids Surf. A. 193 (2001) 145–152.
[38] M. Tanaka, A. Mochizuki, T. Shiroya, T. Motomura, K. Shimura, M. Onishi, Y. Okahata, Colloids Surf. A. 203 (2002) 195–204.
[39] M. Tanaka, A. Mochizuki, N. Ishii, T. Motomura, T. Hatakeyama, Biomacromolecules 3 (2002) 36–41.
[40] M. Ide, T. Mori, K. Ichikawa, H. Kitano, M. Tanaka, A. Mochizuki, H. Oshiyama, W. Mizuno, Langmuir 19 (2003) 429–435.
[41] S. Ye, S. Morita, G. Li, H. Noda, M. Tanaka, K. Uosaki, M. Osawa, Macromolecules 36 (2003) 5694–5703.
[42] M. Tanaka, A. Mochizuki, J. Biomed. Mater. Res. 68A (2004) 684–695.
[43] G. Li, S. Morita, S. Ye, M. Tanaka, M. Osawa, Anal. Chem. 76 (2004) 788–795.
[44] H. Kitano, T. Mori, Y. Takeuchi, S. Tada, M. Gemmei-ide, Y. Yokoyama, M. Tanaka, Macromol. Biosci. 5 (2005) 314–321.
[45] J. Nemoto, Y. Uraki, T. Kishimoto, Y. Sano, R. Funada, N. Obata, H. Yabu, M. Tanaka, M. Shimomura, Bioresour. Technol. 96 (2005) 1955–1958.
[46] H. Kitano, S. Tada, T. Mori, K. Takaha, M. Gemmei-Ide, M. Tanaka, M. Fukuda, Y. Yokoyama, Langmuir 21 (2005) 11932–11939.
[47] E. Hirota, K. Ute, M. Uehara, T. Kitayama, M. Tanaka, A. Mochizuki, J. Biomed. Mater. Res. 76A (2006) 550–560.
[48] Y. Fukuhira, E. Kitazono, T. Hayashi, H. Kaneko, M. Tanaka, M. Shimomura, Y. Sumi, Biomaterials 27 (2006) 1797–1802.

e-J. Surf. Sci. Nanotech. Vol. 3 (2005) 159-164 Conference - Nano-org. & Func. -

Morphological changes in neurons by self-organized patterned films*

Akinori Tsuruma
Graduate School of Science, Hokkaido University, Kita-Ku N11W6, Sapporo 001-0021, Japan

Masaru Tanaka†
Creative Research Initiative 'Sousei', Hokkaido University, Kita-Ku N21W10, Sapporo 001-0021, Japan, and PRESTO, CREST, JST, Honchou 4-1-8, Kawaguchi, 332-0012, Japan

Nobuyuki Fukushima
Graduate School of Medicine, Hokkaido University, Kita-Ku N15W7, Sapporo 060-8638, Japan

Masatsugu Shimomura
Nanotechnology Research Center, Hokkaido University, Kita-Ku N21W10, Sapporo 001-0021, Japan, and CREST, JST, Honchou 4-1-8, Kawaguchi, 332-0012, Japan

(Received 7 April 2005; Accepted 29 April 2005; Published 12 May 2005)

In tissue engineering, micro/nanofabrication is important to modify substrate surfaces for regulating the attachment and growth of cells. In neuroscience, it is significant for neural regeneration; this involves guiding and extending dendrites and axons by a cell culture scaffold which acts as an extra cellular matrix. In this study, we prepared highly regular porous honeycomb-patterned films by a simple casting technique and cultured neurons to investigate their morphologies on the patterned films. The morphologies of neurons were examined by a scanning electron microscope and a confocal laser scanning microscope. The neurons were round and the neurites extended randomly on the flat film. The patterns influenced the morphologies of neurons. The morphologies of neurons were changed by varying the pore size of the honeycomb- patterned films. The neurites spread along the rims of the honeycomb pattern. These results suggest that the self-organized honeycomb-patterned films are useful biomaterials for neural tissue engineering. [DOI: 10.1380/ejssnt.2005.159]

Keywords: Patterning; Neuron; Self-organization; Regenerative medicine; Fabrication; Neural stem cell; Cell differentiation

I. INTRODUCTION

Brain, spinal cord injuries, and neural-degenerative diseases are likely to require the transplantation of neural cells and tissues. The mammalian central nervous system has little capacity for self-repair. The replacement of lost and dysfunctional neurons by tissue transplantation or nerve graft has been investigated [1]. These approaches have been developed as useful tools for restoring function in the damaged central nervous system. In tissue engineering, these approaches are significant for the reconstruction of tissues and organs not only to carry out research on cells or liquid factor but also to develop scaffolds [2, 3]. Scaffolds that have 3-D structures can induce adhesion, proliferation, and differentiation of cells and reorganized tissues and organs. The materials that are used for tissue engineering are made of biodegradable polymers. It has been reported that micro/nano-patterns influenced the morphologies, proliferation, and differentiation of cells [4–6]. It has been found that various micro-patterned substrates fabricated by lithographic techniques can reconstruct artificial neural networks by controlling the morphologies of adhered neurons and outgrowth of neurites [7–13]. These techniques are expected to be applied for neural regeneration in the future. However, these techniques require high energy and involve many processes. In addition, materials for substrates are limited. We have reported that the honeycomb-patterned films are prepared by self-organization [14–16]. The patterned films have regular pores in micro/nano-meter. They can be prepared with ease, low energy, and low cost. Moreover, we can control the pore size of these films. In this study, we cultured neurons on honeycomb-patterned films and investigated the morphological changes in neurons and neurite extension by varying the pore size of the films.

II. EXPERIMENTAL

A. Preparation of self-organized honeycomb-patterned films

Poly (ϵ-caprolactone) (PCL) and an amphiphilic polymer were mixed together and dissolved in chloroform in a weight ratio of 10:1 (Fig. 1(a)). We cast the polymer mixture onto the glass substrates. Honeycomb-patterned films with regular pores were prepared by blowing humid air on the surface of the polymer solution (Fig. 1(b)).

B. Preparation of the PCL flat film

The polymer solution was dropped onto a cover glass. The cover glass with the polymer layer was spun at 1000 rpm for 30 seconds by using a spin coater (MIKASA, 1H-D7).

*This paper was presented at International Symposium on Nano-organization and Function, Tokyo, Japan, 11-12 November, 2004.
†Corresponding author: tanaka@poly.es.hokudai.ac.jp

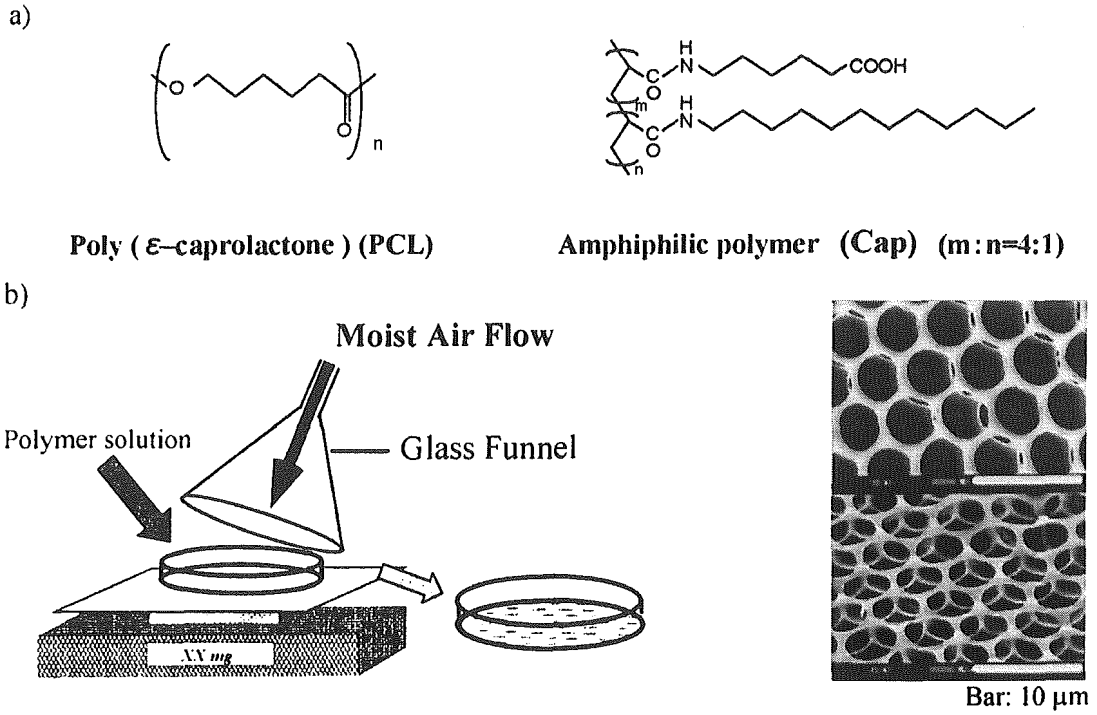

FIG. 1: Preparation of honeycomb-patterned films. a) Chemical structures. b) Casting method.

C. Pretreatment of PCL films

The PCL flat film and PCL honeycomb-patterned films were soaked in 1-propanol solution for 5 minutes and then washed with ethanol. The PCL films were then attached to a cover glass, placed in culture dishes, and sterilized by exposure to UV rays. These films were then soaked in poly-L-lysine solution (50 mg / L, 0.1 M Boric acid, pH 8.3) for 1 hour to coat poly-L-lysine on the films.

D. Preparation of neural cells

Neural cells were prepared from the cerebral cortices of embryonic day-14 mice (CLEA Japan, Inc). In brief, the cerebral cortexes of embryonic day-14 mice were dissected and the meninges were carefully removed. The tissues were transferred into 15-ml tubes with culture medium containing 55 μM 2-mercaptoethanol and gently triturated with a fire-polished pasteur pipette until most of the tissues were dissociated into single cells. The cell number and viability were determined. Cells were seeded onto the PCL flat film to estimate the population of neural stem cells (NSCs). After incubating the cells for 6 hours, cells were immunocytochemically stained for nestin to identify and estimate their population.

E. Cell culture condition

The neural cells were seeded onto the PCL flat film and PCL honeycomb-patterned films at a density of 2.0×10^4 cells/cm^2. They were cultured in serum medium (Opti-MEM (Invitrogen), 10% fetal bovine serum, 55 μM 2-mercaptoethanol (Invitrogen)) for the first day. After the second day, they were cultured in serum-free medium (Opti-MEM, B27 supplement, 55 μM 2-mercaptoethanol). They were incubated at 37°C under a humidified atmosphere of 5% CO_2 .

F. Scanning electron microscopic observation

The cultured cells were fixed with 2.5% glutaraldehyde in phosphate-buffered saline (PBS). They were washed with PBS and water. Subsequently, the samples were dehydrated by washing in increasing ethanol concentrations and then air-dried. The samples were sputtered with platinum and investigated with a scanning electron microscope (Hitachi, S-3500).

G. Immunocytochemistry

1. Immunostaining for β-tubulin III

The cultured cells were fixed with 10% formalin in PBS for 30 minutes at room temperature. The samples were washed with PBS 3 times for 5 minutes. They were then incubated in blocking solution (5% goat serum, 0.2% Triton X-100 in PBS) for 1 hour. Then, the samples were incubated with mouse monoclonal anti-β-tubulin III (1:500) in PBS for 2 hours. After washing with PBS, the samples were incubated with fluorescein isothiocyanate (FITC)-conjugated anti-mouse IgG (1:200) for 2 hours. After washing with PBS and water, the samples were air-dried

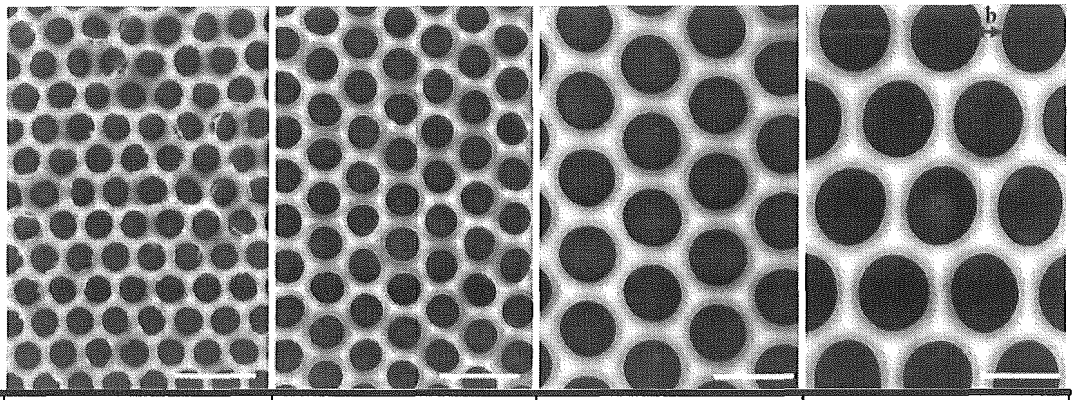

a) Pore size (μm) a	3.2 (± 0.09)	5.1 (± 0.05)	8.4 (± 0.03)	10.2 (± 0.10)
b) Rim size (μm) b	1.1 (± 0.04)	1.3 (± 0.07)	2.8 (± 0.17)	3.8 (± 0.09)
c) Porosity (%)	49.7 (± 2.54)	49.8 (± 1.93)	51.3 (± 3.87)	52.6 (± 2.96)

FIG. 2: SEM images of honeycomb patterned films. a) Pore size, b) Rim size, c) Porosity. Bar=10 μm

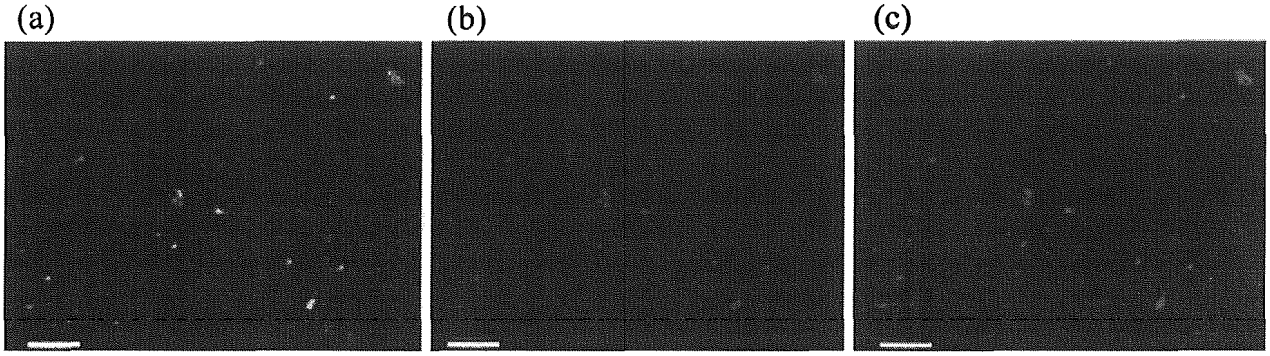

FIG. 3: Population of neural stem cells on PCL flat film after 6 hours culture. (a) Staining with phalloidin and nestin. (b) Staining with phalloidin. (c) Staining with nestin. Bar=100 μm

and then mounted with mounting media for focal microscopic observation.

2. Immunostaining for nestin

The cultured cells were fixed with 10% formalin in PBS for 30 minutes at room temperature. The samples were washed with PBS 3 times for 5 minutes. They were then incubated in blocking solution (5% goat serum, 0.2% Triton X-100 in PBS) for 1 hour. Then, they were incubated with mouse monoclonal anti-nestin (1:1000) in PBS for 2 hours. After washing with PBS, the cells were incubated with biotinylated anti-mouse IgG (1:1000) for 2 hours at 37°C. Then, they were incubated with Alexa 488-conjugated avidin (1:2000) and Texas-red conjugated phalloidin (1:50) for 2 hours at 37°C. After washing with PBS and water, the samples were air-dried and then mounted with mounting media for confocal microscopic observation.

III. RESULTS AND DISCUSSION

A. Preparation of self-organized honeycomb-patterned films

We could prepare self-organized honeycomb-patterned films by casting a polymer solution. The pore size could be controlled in the range from 3 to 10 μm by changing the casting volume [16]. We prepared PCL flat films and PCL patterned films (3 μm, 5 μm, 8 μm, and 10 μm in diameter) for culturing neural cells.

The rims of the honeycomb-patterned films widened with increasing pore size of the patterned films. The porosity of each film was about 50% (Fig. 2).

B. Cell preparation from cerebral cortexes of embryonic mice

The viability of neural cells prepared from the cerebral cortices of 4 mice (embryonic day-14) was 90~95%. We

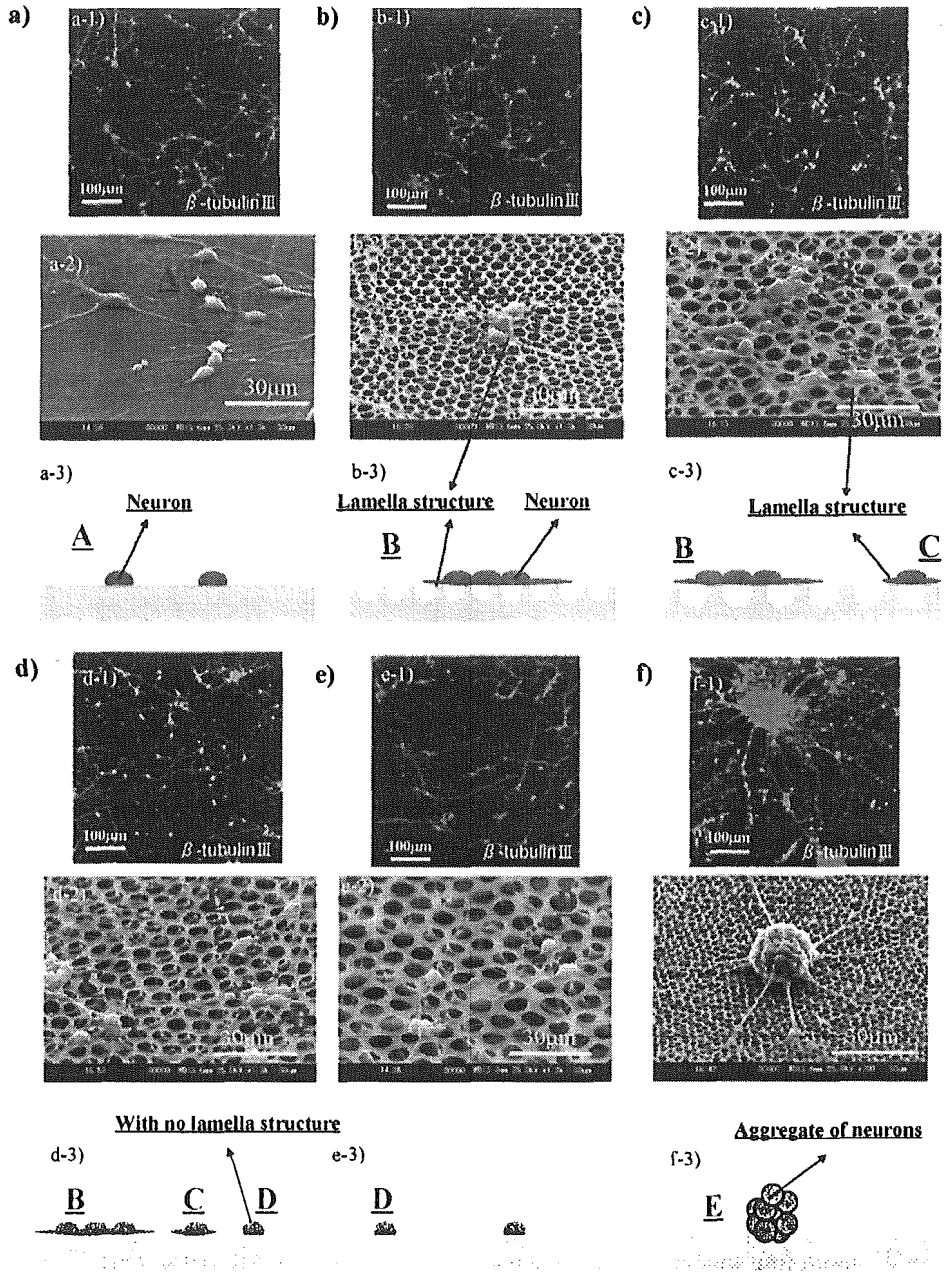

FIG. 4: SEM and confocal images of adhered neurons on PCL film and PCL honeycomb-patterned films after 5 days culture. a-1), b-1), c-1), d-1), e-1), f-1) : Confocal images. a-2), b-2), c-2), d-2), e-2), f-2) : SEM images. a-3), b-3), c-3), d-3), e-3), f-3) : Schematic representations. a) Flat film. Pore size: b) 3 μm, c) 5 μm, d) 8 μm, e) 10 μm, f) 3 μm.

investigated the population of neural NSCs in the prepared cells by staining with nestin. We found that the cell mixture contained 90∼95% of NSCs (Fig. 3).

C. Morphologies of adhered neural cells and neural extension

After 5 days of culture, we investigated the morphologies of adhered neural cells and the extension of neurites on both PCL flat films and PCL honeycomb-patterned films. The neurons were stained for β-tubulin III, a neuron-specific tubulin for their identification and for the observation of neural networks on the films (Figs. 4 (a1)-(f1)).

The neurons possessed highly branched, multi-polar neurites and rounded cell bodies (Fig. 4(a)). On the other hand, several neurons aggregated near each other and adhered with lamella structure around the cell body on the patterned film (pattern pore size: ϕ3 μm) (Fig. 4(b)). Single neurons adhered with lamella structure on the patterned film (pattern pore size: ϕ5 μm) (Fig. 4(c)). The neurons were round with no lamella structure on the patterned film (pattern pore size: ϕ8 μm) (Fig. 4(d)). The neurites extended along the honeycomb-pattern rims and neurons formed network structures on the patterned